Potential of mean force between a spherical particle suspended in a nematic liquid crystal and a substrate: Sphere size effects

Evelina B. Kim and Juan J. de Pablo
Department of Chemical and Biological Engineering, University of Wisconsin, Madison, Wisconsin 53706, USA
(Received 30 May 2003; published 2 June 2004)

The expanded ensemble density of states method (ExEDOS) is used to investigate the effective interaction of a spherical colloidal particle suspended in a confined liquid crystal (LC) with a substrate. The potential of mean force (PMF) is determined as a function of the normal distance between the particle and the substrate's surface. The presence of the substrate induces a layered structure of the LC, which in turn greatly influences the PMF. We analyze the structure of the Saturn ring defect that accompanies the colloidal sphere, and find that the ring is displaced slightly towards the surface when the sphere is within the first LC surface layer. A transition occurs from an overall attraction of the colloid to the substrate to a global repulsion when the sphere's radius is roughly twice the length of the LC molecules.

DOI: 10.1103/PhysRevE.69.061703 PACS number(s): 61.30.Hn, 61.30.Jf

I. INTRODUCTION

Suspensions of colloidal particles in nematic liquid crystals (LCs), bulk or confined, exhibit a number of interesting characteristics; these include the formation of topological defects and the occurrence of anisotropic interactions between colloidal particles. Several studies have considered these phenomena from both the experimental [1–3] and theoretical points of view [4–8]. While these studies have focused on micrometer length scales, a number of more recent publications has appeared that probed the nanometer scale aspect of the problem through the use of molecular dynamics simulations [9–12].

The alignment of liquid crystalline (LC) films on a substrate is remarkably sensitive to surface chemistry and nanometer scale topography. Self-assembled monolayers (SAM) of alkanethiols chemisorbed on obliquely deposited gold films exhibit well-defined surface chemistry and topography and are uniquely suited to investigate the response of LCs to surface characteristics [13]. These surfaces can be used to induce a uniform alignment of the LC extending over tens of microns. The specific binding of proteins or viruses to bio-receptors embedded in SAMs distorts the local nematic order; this perturbation is further amplified into the bulk and results in the formation of multidomains that can be detected with an optical microscope. This ability of LCs to optically amplify and transduce binding events at surfaces has been employed to design LC-based bio-sensors [14,15].

In a bio-sensor, a binding of a protein is detected through the formation of topological defects triggered by distortion of local nematic field at the binding site. The size of the proteins in these experimental sensors ranges from 3 to 5 nm [14,15] (compare that to the length of a typical LC former, e.g. pentylcyanobiphenyl 5CB at 1.8 nm); the shape (or conformation) of these proteins is largely globular. A better understanding of the perturbation of the nematic field by a protein could lead to effective designs for such sensors. While we would benefit considerably from atomistic-level simulations of proteins suspended in liquid crystals, calculations of that magnitude would require extraordinary computational resources. A reasonable compromise between molecular-level resolution and computational feasibility can be achieved by resorting to a coarse-grained model. In this work we model liquid crystal molecules as Gay-Berne ellipsoids, and we examine how spherical particles of different sizes interact with a substrate through the liquid crystal. By adopting such a model, we are able to examine the effects of the shape, size, and anchoring properties of the colloids and their interactions with surfaces at a molecular level. Molecular simulations provide unique insights regarding phenomena at the nanometer scale and they do not require any assumptions (other than those implicit in the choice of a model or force field), thereby providing an ideal complement to studies involving continuum and field theories (and thus strictly valid only at macro- or mesoscopic length scales).

II. SIMULATION METHODS

The system under consideration consists of N liquid crystal particles confined by two soft repulsive walls at $z=0$ and $z=Z_{\text{wall}}$. A soft repulsive sphere of radius R is separated from the lower surface by a distance z_{sph} [see Fig. 1(a)]; z_{sph} plays the role of a reaction coordinate ξ. A recently proposed expanded ensemble density of states method (ExEDOS) is used in this work to perform the free energy or potential of mean force (PMF) calculations. This method offers advantages in that it facilitates good sampling of phase space without prior knowledge of the energy landscape of the system.

In accordance with the expanded ensemble technique, the reaction coordinate is discretized or expanded; an expanded state m [see Fig. 1(b)] is defined as

$$m^{\text{th}}\ \text{state} \equiv (m-1)\,\Delta z + z_{\text{sph}}^{\text{ref}} \leqslant z_{\text{sph}} < m\,\Delta z + z_{\text{sph}}^{\text{ref}}, \quad (1)$$

where the reference value of $z_{\text{sph}}^{\text{ref}}$ defines the lower boundary for the reaction coordinate. If M such states are introduced, the partition function for the entire system at constant number of particles N, volume V, and temperature T is given by

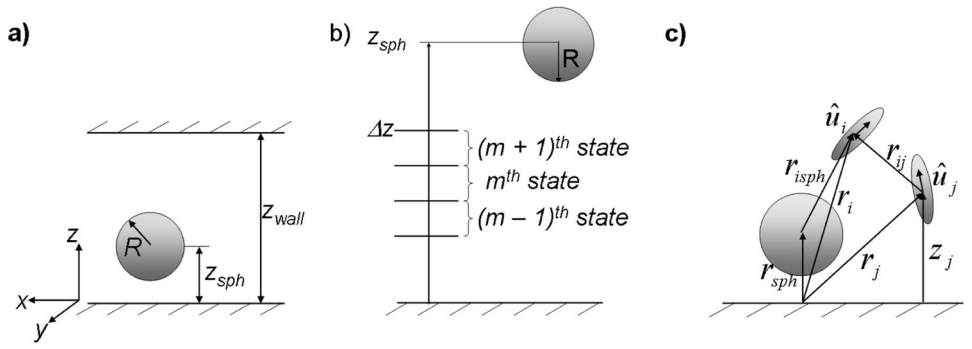

FIG. 1. (a) Schematic view of the system. (b) Definition of the expanded states. (c) Various interactions between the LC particles and the colloid and the substrate.

$$\Omega = \sum_{m=1}^{M} Q(N,V,T,m) g_m = \sum_{m=1}^{M} Q_m g_m, \tag{2}$$

where Q_m and g_m designate a partition function and a weighting factor for a state m, respectively. The partition function is related to the free energy or PMF, $w(\xi_m)$, of the system through the following expression:

$$\beta w(\xi_m) = -\ln Q_m. \tag{3}$$

If the weight factors are equal to $1/Q_m$ the probability of visiting a state m becomes uniform and proportional to $1/\Omega$. In that case, the PMF can be obtained from the known $1/g_m$. By designing an algorithm that ensures equally probable visits to all states, one can ensure that the weighting factors, g_m, provide a faithful estimate of the inverse density of states, Q_m. The PMF is then obtained from

$$\beta[w^{\mathrm{wt}}(z_{\mathrm{sph},m}) - w^{\mathrm{wt}}(z_{\mathrm{sph},1})] = -\ln \frac{Q_m}{Q_1} = [\ln g_m - \ln g_1]. \tag{4}$$

Only a brief outline of the algorithm employed to achieve uniform state sampling is provided here. Details can be found in [16,17]. Every time a state m is visited (i.e., whenever the z coordinate of the sphere changes) the weight g_m is modified by an arbitrary convergence factor f according to

$$g_m \rightarrow g_m / f, \tag{5}$$

and the histogram of visits to that state is updated. The acceptance criteria for changing from an *old* state to a *new* state are given by

$$\begin{aligned} P_{\mathrm{acc}}(\mathrm{old} \rightarrow \mathrm{new}) &= \min\{1,\ \exp[-\beta(U_{\mathrm{new}} - U_{\mathrm{old}}) \\ &\quad + (\ln g_{\mathrm{new}} - \ln g_{\mathrm{old}})]\} \\ &= \min\{1,\ \exp[-\beta \Delta U + \Delta \ln g]\}. \end{aligned} \tag{6}$$

Once a global histogram for a given value of f is sufficiently flat (the minimum histogram entry being at least 85% of the average), f is decreased according to a monotonically decreasing function (the square root is commonly used). The random walk cycle then resumes with a smaller value of f. The simulation proceeds until f falls below a certain threshold value. In traditional DOS simulations, threshold values of 10^{-7} to 10^{-8} are enforced to achieve an acceptable accuracy for the density of states. In this application much less stringent values (10^{-2} to 10^{-3}) are sufficient. In particular, the initial value of $\ln f$ was set at 0.1 (all $\ln g_m$ were initialized to the same value of 0.1 at the beginning of a simulation); it was halved four times to a final value of 0.00625.

The PMF can also be obtained independently by measuring and integrating the mean force F_{sph} as a function of z_{sph},

$$w^{\mathrm{force}}(z_{\mathrm{sph},m}) - w^{\mathrm{force}}(z_{\mathrm{sph},1}) = \int_{z_{\mathrm{sph},1}}^{z_{\mathrm{sph},m}} F_{\mathrm{sph}}(z)\,dz. \tag{7}$$

The mean force is a simple average of the resultant force due to the interactions between the colloidal sphere and the LC molecules within the cutoff radius of the sphere. The two independent estimates of the PMF, w^{wt} [Eq. (4)] and w^{force} [Eq. (7)], must agree, and the agreement, in addition to the predetermined threshold value of f, can be used as a criterion for convergence of the weights g_m.

Since the two final PMF curves w^{wt} and w^{force} are in close agreement, we present only the latter as the results for the PMF in Sec. IV. The reason for our choice is that the integration of the force yields a smoother curve than that obtained from the weights g_m.

III. SIMULATION DETAILS

The system under study comprises at least 11 460 (14 500 for the largest sphere) liquid crystal particles confined between two soft repulsive walls at $z=0$ and $z=Z_{\mathrm{wall}}$. The LC particles are represented by soft repulsive ellipsoids of revolution having length to width (σ_0) ratio κ of 3. Each molecule i is characterized by a center of mass position vector $\boldsymbol{r}_i$ and an orientation unit vector $\hat{\boldsymbol{u}}_i$. Mesogens i and j interact along an intermolecular vector $\boldsymbol{r}_{ij}=\boldsymbol{r}_i-\boldsymbol{r}_j(|\hat{\boldsymbol{r}}_{ij}|=1)$ via a shifted and truncated Gay-Berne (GB) potential,

$$U_{ij} = \begin{cases} 4\varepsilon_0(\varrho_{ij}^{-12} - \varrho_{ij}^{-6}) + \varepsilon_0, & \varrho_{ij}^6 < 2 \\ 0, & \varrho_{ij}^6 > 2 \end{cases} \tag{8}$$

$$\varrho_{ij} = (|\boldsymbol{r}_{ij}| - \sigma_{ij} + \sigma_0)/\sigma_0, \tag{9}$$

$$\sigma_{ij} = \sigma_o \left[1 - \frac{\chi}{2} \left\{ \frac{(\hat{\boldsymbol{r}}_{ij} \cdot \hat{\boldsymbol{u}}_i + \hat{\boldsymbol{r}}_{ij} \cdot \hat{\boldsymbol{u}}_j)^2}{1 + \chi \hat{\boldsymbol{u}}_i \cdot \hat{\boldsymbol{u}}_j} + \frac{(\hat{\boldsymbol{r}}_{ij} \cdot \hat{\boldsymbol{u}}_i - \hat{\boldsymbol{r}}_{ij} \cdot \hat{\boldsymbol{u}}_j)^2}{1 - \chi \hat{\boldsymbol{u}}_i \cdot \hat{\boldsymbol{u}}_j} \right\} \right]^{-1/2}, \tag{10}$$

$$\chi = \frac{\kappa^2 - 1}{\kappa^2 + 1}, \tag{11}$$

where σ_{ij} describes a contact distance between a pair of ellipsoids i and j, and σ_0 and ε_0 are length and energy parameters.

In addition, the LCs interact with all interfaces according to the same potential as in Eq. (8), with ϱ_{ij} defined differently for a sphere and a surface:

$$\varrho_{ij} = (|\boldsymbol{r}_i - \boldsymbol{r}_{\mathrm{sph}}| - R + \sigma_0/2)/\sigma_0, \tag{12}$$

$$\varrho_{ij} = (|z_i| + \sigma_o/2)/\sigma_0. \tag{13}$$

In this case, $\boldsymbol{r}_{\mathrm{sph}}$ and $|z_i|$ denote the position vector for the center of mass of the sphere of radius R and the normal distance of a mesogen i from a surface, respectively. These potentials result in homeotropic (perpendicular) anchoring of LC molecules at all interfaces. The force on a sphere due to a given mesogen is calculated as the derivative of the interaction potential between the liquid crystal and the sphere with respect to z; due to symmetry in the (x,y) plane, only the z component of the force contributes to the total force. The surface and sphere interact as hard bodies: the minimum distance possible between a surface and the center of mass of the sphere is the radius of the sphere. In this work the radius of the sphere was varied from $3\sigma_0$ to $6\sigma_0$, while the separation between the walls was set at $Z_{\mathrm{wall}} = 34\sigma_0$.

Simulations were conducted at a reduced temperature $T^* = kT/\varepsilon_0 = 1.0$ and density $\rho^* = N\sigma_0^3/V = 0.335$. All variables henceforth are reduced with respect to the length and energy parameters σ_0 and ε_0 and the superscripts are dropped for brevity. The simulation box is rectangular with side lengths equal in the x and y directions. Periodic boundary conditions are used in the x and y directions.

Before proceeding with this system, we emphasize the importance of the structure of the LC in a confined system in the absence of a colloid: as was pointed out earlier [16], it is this structure that largely determines the nature of the interactions between the colloid and a substrate. Figure 2 shows the density and second rank order parameter (P_2) profiles for a confined system obtained from an independent simulation. Here P_2 is the largest eigenvalue of the order parameter tensor $\mathbf{Q}$ calculated from the orientations $\hat{\boldsymbol{u}}_i$ of N_V particles in a sample volume as

$$\mathbf{Q} = \frac{1}{N_v} \sum_{i=1}^{N_V} \left(\frac{3}{2} \hat{\boldsymbol{u}}_i \hat{\boldsymbol{u}}_i - \frac{1}{2} \mathbf{I} \right), \tag{14}$$

where $\mathbf{I}$ denotes the identity tensor. The eigenvector $\mathbf{n}$ associated with P_2 is the director or the average orientation of the N_V particles.

From Fig. 2 one can see that several layers are formed at the surface. In the midsection the density and P_2 profiles are relatively flat. In this work we are mostly concerned with the molecular-level structure of the colloidal-liquid crystal system; we expect strong features to arise in the immediate vicinity of the surface and much weaker, bulklike structure in the midsection of the system, i.e., a relatively flat PMF profile. It is therefore reasonable to set the range of z_{sph} between a lower boundary equal to the radius of the sphere and an upper boundary of 13—15. From a computational point of view this range is rather large, particularly considering that the separation between the states, Δz, must be small for accurate integration of the mean force. For our choice of Δz of 0.01, the entire range of the reaction coordinate was divided into fully overlapping windows of width 2, i.e., each window consists of $M = 200$ states in a segment $[z_{\mathrm{sph},1}, z_{\mathrm{sph},1} + 2]$. A move to a new state, i.e., a move of a sphere in the z direction (its x and y coordinates are kept at zero throughout the entire simulation), is attempted every Monte Carlo cycle; a cycle consists of a trial move for all liquid crystal molecules.

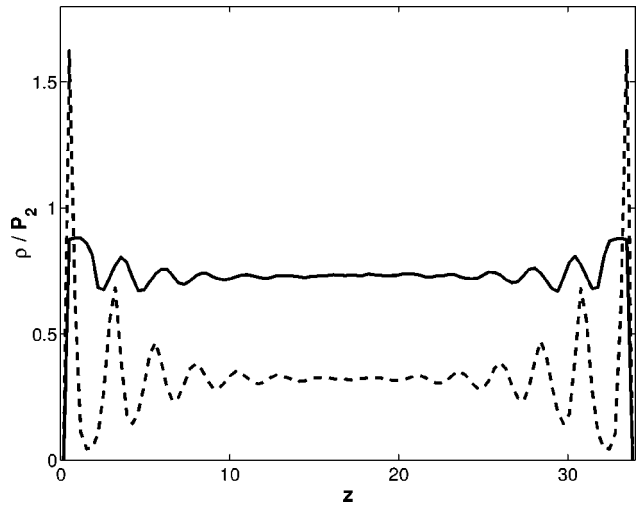

FIG. 2. Density (dashed line) and P_2 (solid line) profiles for a confined system.

IV. RESULTS AND DISCUSSION

Figure 3 shows results for the mean force, and Fig. 4 shows the corresponding potential of mean force for spheres of different sizes. The key variable for characterization of the interactions between a sphere and the substrate is the distance between the surface of the substrate and the surface of the sphere, $s = z_{\mathrm{sph}} - R$. With this choice of reaction coordinate, the PMF and mean force profiles collapse nicely in terms of the local minima and maxima. Moreover, when a density profile $\rho(z)$ for a confined system (in the absence of a colloid) is superimposed on the PMF profiles, the peaks of $\rho(z)$ coincide with the spheres minima in the PMF curves, indicating that the preferential separation between the substrate and the spheres' surfaces is such that the latter coincide with the middle of dense surface LC layers; this interpretation differs from one adopted in a previous publication [1].

For the separation between walls considered here, $Z_{\mathrm{wall}} = 34$, in the absence of the colloid one can identify a bulk region, where the LC does not exhibit any structure (namely, the $P_2(z)$ and $\rho(z)$ profiles are flat, as in Fig. 2). This bulk

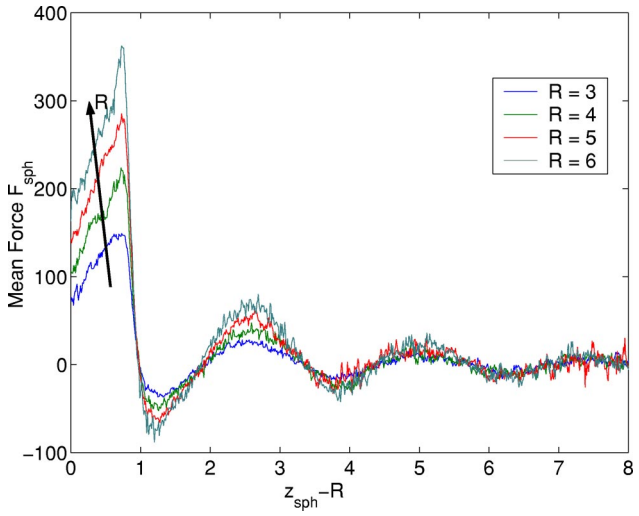

FIG. 3. Mean force acting on colloidal spheres of radii in the range 3—6. The arrow indicates an increasing radius.

region spans the interval $13 \leqslant z \leqslant 21$. To avoid or minimize finite-size effects in the computation of the PMF between a colloid and a wall, the bulk region must be large enough to accommodate an entire colloid, so that its surface is sufficiently removed from the LC structure-rich region of the second wall. Otherwise, the sphere starts to interact with the second substrate, and the PMF is no longer flat in the middle of the film. This condition is satisfied only for the two smallest radii considered in this work, namely $R=3$ and 4. For $R=5$ and 6, however, this is no longer the case; nonetheless, the PMF can still be calculated for sufficiently small values of s.

It is apparent from Figs. 3 and 4 that the general shape of the mean force F_{sph} and PMF is not affected by the size of a sphere; rather, the extent of repulsion or attraction intensifies with increasing size. For all sizes the mean force is strongly

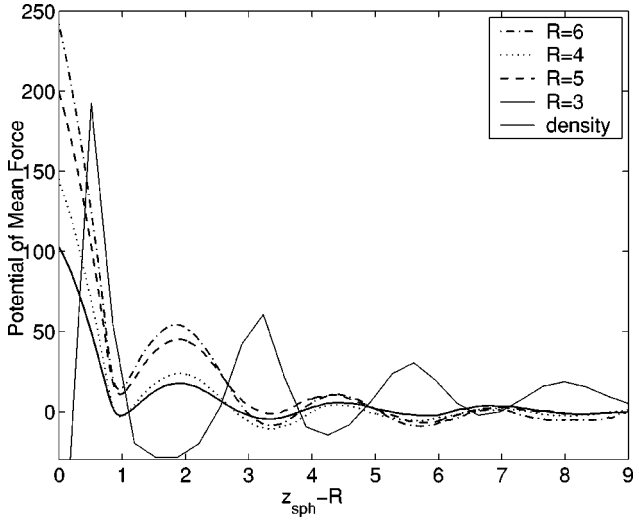

FIG. 4. The potential of mean force between the surface and the spheres of radii 3—6. The density of the confined system without the sphere (solid line) superimposed on the PMF profiles was scaled and shifted along the y axis by an arbitrary amount.

repulsive in the immediate vicinity of the surface, and it reaches a maximum at $s \approx 0.8$. The force then decreases rapidly, dropping to zero at 1 and eventually reaching its minimum value at $s=1.3$. Henceforth the force exhibits a damped oscillatory behavior with a low frequency wavelength of 2.5—2.6, coinciding with the thickness of the LC layers formed at the surface. Force oscillations die out within 2—3 wavelengths, at which point the force becomes effectively zero. Correspondingly, the PMF calculated as the negative integral of F_{sph} is shifted to equal zero at large s and displays peaks and wells with the same frequency as the force profile; the maxima and minima in these oscillations coincide with zeroes of the force.

Quantitatively, the largest difference between the curves for various sphere sizes is observed over the range of $s \in (0,1)$, i.e., the first surface layer of the LC. Clearly, the repulsion at the substrate dominates and dictates the overall character of the interactions between the colloid and the surface. Note that the repulsive force at the substrate increases at a higher rate than that at which the attractive force at $s=1.3$ decreases with the size of the sphere. Since further undulations are virtually indistinguishable in frequency and amplitude, it is the value of the negative integral of F_{sph} over this short range of s that determines the sign of the local minima in the PMF profiles. Eventually, as R increases, these minima adopt positive values compared to the PMF of zero at large s or, in other words, the overall interaction with the substrate becomes repulsive. In fact, we are able to discern this trend in the range of radii considered in this work: spheres of radii of 5 and 6 are clearly repelled by the substrate. We anticipate that for much larger spheres the interactions with the substrate will become prevalently repulsive. Conceivably, in the continuum limit one would expect to observe global repulsive forces — this is indeed the case reported in [4,8], where the interactions between a colloidal sphere and a substrate in the continuum description exhibit a purely repulsive character.

To understand what causes the change in sign for the mean force and, consequently, the character of the PMF profile for $s \geqslant 1$, we analyze the LC density profiles at the values of s corresponding to the first minimum ($s=s_{\min,1}=1$), first maximum ($s=s_{\max,1}=2$), and second minimum ($s=s_{\min,2}=3.3$) in the PMF. To obtain the necessary data, we ran a series of separate *NVT* ensemble simulations with a sphere fixed at the indicated values of s. These simulations were run for 5×10^5 Monte Carlo cycles and trajectories were recorded every 2000 cycles; the initial configurations were extracted from the ExEDOS simulations when $\ln f$ equaled 0.00625. For the analysis of these trajectories we employed the cylindrical symmetry of the system around the axis going through the center of mass of the sphere and perpendicular to the substrate. For each configuration, the LC molecules were rigidly rotated around the axis of symmetry until their center of mass coordinates coincided with the xz plane. A two-dimensional histogram was constructed on a rectangular grid in x and z, and the average number density was calculated for each bin. The resulting density contour maps at the selected positions of the largest sphere are presented in Fig. 5.

As is immediately apparent from the density profiles (see Fig. 5), liquid crystals form a highly dense first layer (corre-

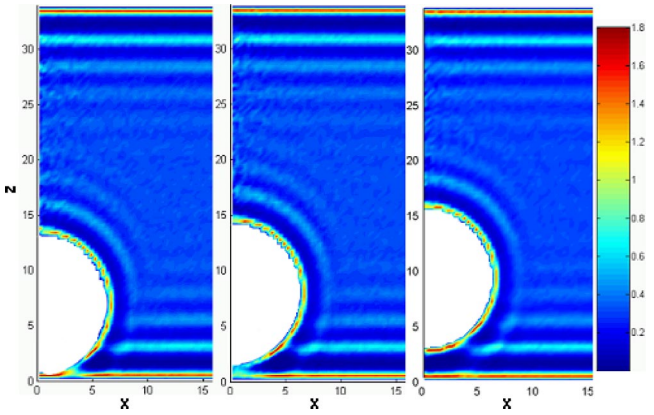

FIG. 5. (Color online) Density contour maps in the *xz* plane at (left to right) the first minimum ($s=1$), first maximum ($s=2$), and second minimum ($s=3.3$) seen in PMF for $R=6$. (See text for details.)

sponding to the red color on the plot) and less dense second layer (light blue) at the surfaces of both the sphere and the substrate. The space between these layers appears dark blue — a density of nearly zero, which translates into virtually no molecular centers of mass present in the corresponding bins. Note that a cavity can be observed in the space where the sphere breaks contact with the substrate and curves away from it. In fact, the first LC layer shared by the sphere and the substrate at $s=1$ is rarified (from the density value of 1.8 to 0.8) where the surfaces break away from each other (150° clockwise from positive vertical axis). This is caused by the molecules' tendency to satisfy anchoring conditions on both surfaces simultaneously — therefore, it is the sphere's curvature that is responsible for breaking the shared dense layer in two. A close inspection shows that the rarified or diffuse region is occupied by the molecules that oscillate between the two surfaces but are still able to satisfy anchoring conditions on both of them; the cavity, however, contains essentially no molecular centers of mass, but, rather, the ends of the molecules from the sphere and substrate surface layers. The "break"-point (along with the cavity) propagates and expands even further as the sphere moves upward. This highest degree of diffusion of the first dense layer corresponds to the maximum in the free energy and a highly unstable state ($s=2$). Moving further along the vertical direction stabilizes the system; the spacing between the substrate and the sphere allows both interfaces to satisfy anchoring conditions by forming exactly two layers ($s=3.3$). Note, however, that at the second minimum, the second, dense surface layer induced by the presence of the substrate is now disturbed by the sphere in the same manner as the first layer was disturbed for $s=1$. This situation repeats itself with each new surface layer until the density profile and the PMF profile become featureless.

The discrepancy between the directions of the molecules dictated by the two interfaces translates into elastic bend energy that is higher in the structured region in the vicinity of the substrate than in the bulk. Therefore, the elastic energy contribution to the PMF is repulsive in character. On the other hand, the attraction between the substrate and a sphere

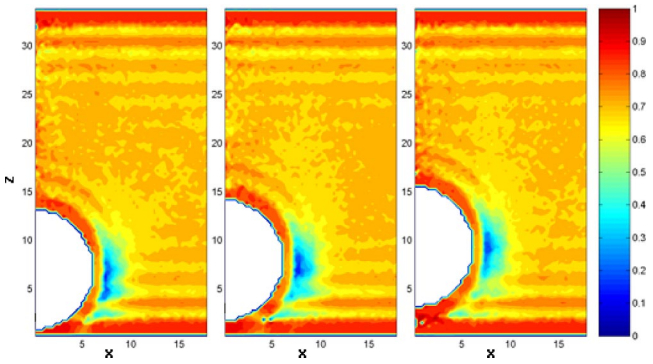

FIG. 6. (Color online) P_2 contour maps in the *xz* plane at (left to right) the first minimum ($s=1$), first maximum ($s=2$), and second minimum ($s=3.3$) seen in PMF for $R=6$. (See text for details.)

is caused by a variation in the liquid crystal density and is entropic in nature. Together, these two contributions result in the observed oscillatory character of the PMF profile.

We next determine how the proximity to the substrate modifies the structure of the Saturn ring defect that is formed around a sphere. For this purpose, we conduct the same analysis as for the density data. This time, however, the **Q** tensor defined in Eq. (14) is collected for each bin. The order parameter P_2 and the director **n** were computed as the largest eigenvalue of the order parameter tensor and the eigenvector associated with it, respectively. The resulting P_2 contour map as well as the director profile at the selected positions of the largest sphere are presented in Fig. 6 and 7. Dispersion of spherical particles in the liquid crystal is accompanied by the formation of topological defects, such as the Saturn ring disclination line defect and the hedgehog point defect. The stability of these defects depends on the size of the droplets and the confinement conditions (see Ref. [8] and references therein). In our simulated system, we observe the formation of Saturn ring defects in the bulk and under confinement. The Saturn ring disclination line is described by a circumference in the equatorial plane of a spherical particle and represents the points in space where the director field is discontinuous. For example, the director profile on the utmost right panel in Fig. 7 illustrates the location of the disclination line

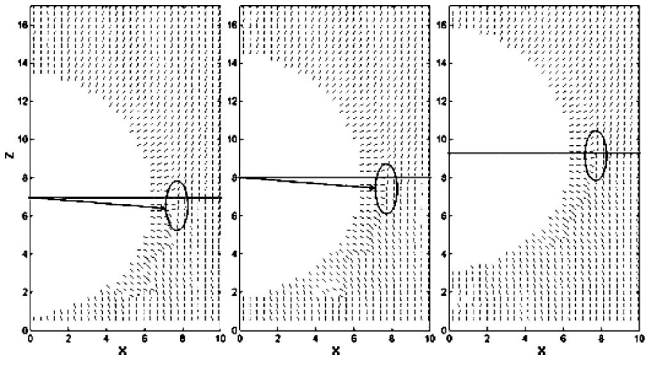

FIG. 7. Director profiles in the *xz* plane at (left to right) the first minimum ($s=1$), first maximum ($s=2$), and second minimum ($s=3.3$) seen in PMF for $R=6$. Drawn circles indicate the Saturn ring defect cores; the arrows indicate deviations from the equatorial plane.

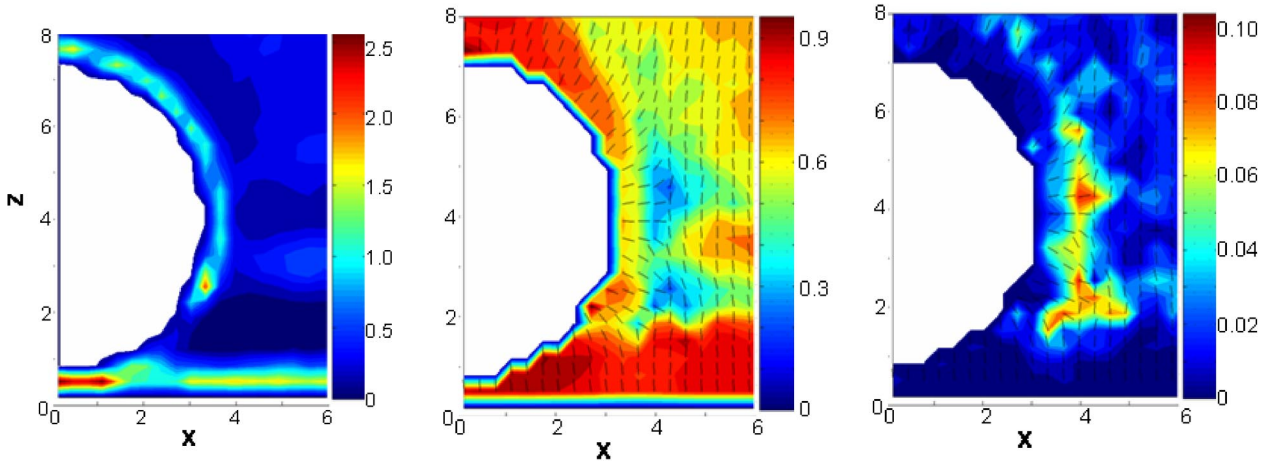

FIG. 8. (Color online) Left to right: density, P_2, and biaxiality maps with the superimposed director profile in the xz plane for the sphere of $R=3$ at the separation $s=1$.

in the middle of a drawn circle. The director discontinuity is caused by the abrupt change in preferred molecular orientations at the surface of the sphere (horizontal) and in the bulk (vertical). Consequently, the defect is characterized by low molecular coalignment P_2 and high biaxiality.

The order parameter maps shown in Fig. 6 indicate a layered structure of the LC near the substrate; P_2 varies from 0.95 in the middle of the layer to 0.65 in between the layers. The blue color seen around the equatorial plane of the sphere indicates the presence of the Saturn ring disclination line. The earlobe-shaped region of low P_2 associated with the defect is stretched towards the substrate as the sphere approaches its surface (see also Fig. 7). Also note that highly oriented substrate surface layers of LC molecules (red or orange) cut into the defect (blue) region, thereby slicing off areas with anomalously low P_2 (cyan blue color corresponding to $P_2 \approx 0.4$). This process is enabled by the presence of highly dense and highly oriented first and second substrate-induced surface layers, whose vertical orientation conflicts with the tilted orientation of the sphere-induced surface layer. As discussed above, these regions are characterized by low molecular centers of mass occupancy as molecules preferentially reside in a surface layer rather than in between the layers. It must be pointed out that the third and fourth substrate-induced surface layers are significantly weakened (much lower density and P_2 variation), and do not affect the shape of the defect region.

For the larger spheres considered here, i.e. $R=5,6$, the equatorial plane around which the Saturn ring resides is above the first two strongly expressed layers. For smaller spheres, the equatorial plane is roughly at the same level as these two first layers and, hence, the distortion of the defect region is enhanced, especially when the sphere is close to the substrate. For comparison with the largest sphere, we plotted the density, order parameter, and biaxiality maps for $R=3$ at $s=1$ in Fig. 8. Here biaxiality is defined as a third of the difference between the middle-valued and the smallest eigenvalues of the **Q** tensor [see Eq. (14)]. The location of a defect is taken as a minimum in P_2 and a maximum in biaxiality. What distinguishes the order parameter map in this case is that the "sliced-off" area of low P_2 displays values as low as those seen in the Saturn ring defect core. Still, as in the case of the largest sphere, the equatorial low P_2 region is associated with the Saturn ring defect, while the lower one corresponds to a cavity observed in the corresponding density profile. Higher degree of disordering, i.e., lower P_2 and higher biaxiality in this latter region, is due to the higher curvature of small spheres. LC molecules have little space to undergo the orientational change caused by a difference in anchoring. This is illustrated by the snapshots of the system in Fig. 9 for the cases of $R=3$ and $R=6$. In the former case, LC molecules change their orientation almost in a discrete manner from vertical at the substrate to horizontal at the sphere surface, whereas in the latter, the orientational change is comparatively smooth.

Another feature that distinguishes large $(R=5,6)$ and small $(R=3,4)$ spheres is that the Saturn ring defect is displaced slightly towards the surface for the former, but not for the latter. Deviations of the defect from the equatorial plane are shown by the arrows in the case of the largest sphere in Fig. 7. The smectic layers formed at the substrate have a higher resistance to bending, i.e., a higher elastic energy, than the unstructured bulk nematic fluid. This change in the elastic properties of the LC occurs over a short distance and is a likely cause of the Saturn ring being pulled towards the substrate from the equatorial plane of the particle to mini-

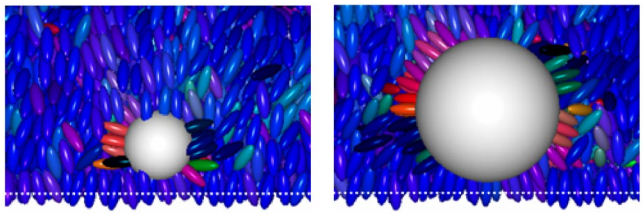

FIG. 9. (Color online) Formation of the Saturn ring defect around the smallest ($R=3$, left) and largest ($R=6$, right) spheres at $s=1$. The LC molecules are color-coded according to their orientation with the blue coinciding with the vertical axis; white dotted line indicates the wall at $z=0$.

mize the bending energy. This effect is observed only for the large spheres whose equatorial plane is in proximity of the structured LC region. For small spheres, this effect is much less pronounced due to the smaller spherical surface as well as the length of the disclination line.

The lower elastic (repulsive) energy contributions for small spheres are consistent with the PMF profiles: while the PMF curves for $R=3$ and 4 differ mainly in the repulsive energy at the substrate $[w(s_{\min,1})-w(0)]$, in both cases the first two minima are below zero. In contrast, the PMF curves for larger radii "lift off" with their positive local minima and give an overall repulsive character to the sphere-substrate interactions. Therefore, it is plausible to conclude that this change from repulsive to slightly attractive or neutral behavior takes place when LC molecules are of the order of the radius of a sphere. We find that two layers away from the surface the disclination line is not attracted to the substrate for all four sphere sizes examined in this work.

V. CONCLUSION

We have applied the recently developed ExEDOS Monte Carlo simulation method to study the behavior of spherical colloidal particles dispersed in confined liquid crystal. In this work we examined in detail the effect of colloid size on its effective, LC-mediated interaction with the substrate. In particular, free energy profiles were obtained by integrating the mean force as a function of the sphere separation from the surface. The layered structure of the LC near surfaces profoundly influences the mean force (and the potential of mean force) on the sphere. Liquid crystal layers (or oscillations in the density profile) of the confined system give rise to out-of-phase undulations in the PMF profiles, and reveal the sphere's preference to reside in the middle of the layers. The energy is lower when the spacing between the substrate and the surface of the sphere is such that an integer number of LC layers of characteristic thickness can be accommodated. Once the solvent density loses structure, approximately four layers away from the surface, the PMF and mean force curves become featureless. From the free energy profiles we are able to discern a qualitative change in the interactions between a sphere and the substrate when the radius of the sphere is roughly twice the length of a liquid crystal molecule ($R=5-6$). Most notably, the slight attraction to the substrate switches to global repulsion. This is consistent with the observation of purely repulsive forces between a colloidal sphere and a substrate in a continuum description [4,8]. In addition, when the separation between the interfaces is $s=1$, the Saturn ring defect that accompanies larger spheres ($R=5,6$) is displaced slightly towards the substrate. In the case of the two smallest spheres considered here, an additional anomaly may be observed. The abruptness with which the molecules change their orientations in their tendency to satisfy anchoring homeotropic conditions on both interfaces in the region where sphere and substrate meet is responsible for this anomaly.

ACKNOWLEDGMENTS

This work has been supported by the University of Wisconsin Materials Research Science and Engineering Center on Nanostructured Materials and Interfaces (NSF-DMR-0079983). E.B.K. is indebted to Roland Faller, Sylvain Grollau, and Orlando Guzmán for stimulating discussions and valuable suggestions concerning this work.

[1] Philippe Poulin, Holger Stark, T. C. Lubensky, and D. A. Weitz, Science **275**, 1770 (1997).
[2] P. Poulin and D. A. Weitz, Phys. Rev. E **57**, 626 (1998).
[3] Yuedong Gu and Nicholas L. Abbott, Phys. Rev. Lett. **85**, 4719 (2000).
[4] E. M. Terentjev, Phys. Rev. E **51**, 1330 (1995).
[5] R. W. Ruhwandl and E. M. Terentjev, Phys. Rev. E **55**, 2958 (1997).
[6] H. Stark, Eur. Phys. J. B **10**, 515 (1999).
[7] M. Tasinkevych, N. M. Sylvestre, P. Patricio, and M. M. Telo da Gama, Eur. Phys. J. B **9**, 341 (2002).
[8] Sylvain Grollau, N. L. Abbott, and J. J. de Pablo, Phys. Rev. E **67**, 011702 (2003).
[9] Jeffrey L. Billeter and Robert A. Pelcovits, Phys. Rev. E **62**, 711 (2000).
[10] Denis Andrienko, Guido Germano, and Michael P. Allen, Phys. Rev. E **63**, 041701 (2001).
[11] Denis Andrienko, Michael P. Allen, Gregor Skacej, and Slobodan Zumer, Phys. Rev. E **65**, 041702 (2002).
[12] Denis Andrienko, M. Tasinkevych, P. Patricio, Michael P. Allen, and M. M. Telo da Gama, Phys. Rev. E **68**, 051702 (2003).
[13] Justin J. Skaife, Jeffery M. Brake, and Nicholas L. Abbott, Langmuir **17**, 5448 (2001).
[14] Vinay K. Gupta, Justin J. Skaife, Timothy B. Dubrovsky, and Nicholas L. Abbott, Science **279**, 2077 (1998).
[15] John A. Van Nelson, Seung-Ryeol Kim, and Nicholas L. Abbott, Langmuir **18**, 5031 2002.
[16] Evelina B. Kim, Roland Faller, Qiliang Yan, Nicholas L. Abbott, and Juan J. de Pablo, J. Chem. Phys. **117**, 7781 (2002).
[17] F. Calvo, Mol. Phys. **100**, 3421 (2002).